THE JOURNAL OF PHYSICAL CHEMISTRY Letters

pubs.acs.org/JPCL

Letter

Strong Electric Field Observed at the Interface of Aqueous Microdroplets

Hanqing Xiong, Jae Kyoo Lee, Richard N. Zare,* and Wei Min*

Cite This: *J. Phys. Chem. Lett.* 2020, 11, 7423−7428

Read Online

ACCESS | Metrics & More | Article Recommendations | Supporting Information

ABSTRACT: Chemical reactions in aqueous microdroplets often exhibit unusual kinetic and thermodynamic properties not observed in bulk solution. While an electric field has been implicated at the water interface, there has been no direct measurement in aqueous microdroplets, largely due to the lack of proper measurement tools. Herein, we employ newly developed stimulated Raman excited fluorescence microscopy to measure the electric field at the water−oil interface of microdroplets. As determined by the vibrational Stark effect of a nitrile-bearing fluorescent probe, the strength of the electric field is found to be on the order of 10^7 V/cm. This strong electric field aligns probe dipoles with respect to the interface. The formation of the electric field likely arises from charge separation caused by the adsorption of negative ions at the water−oil interface of microdroplets. We suggest that this strong electric field might account in part for the unique properties of chemical reactions reported in microdroplets.

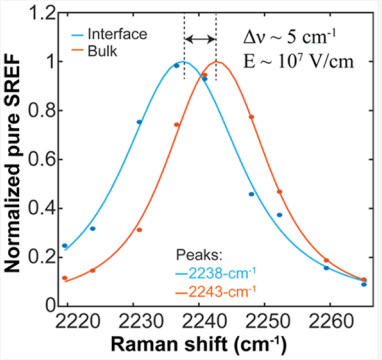

Properties of molecules and chemical reactions in microdroplets often differ significantly from those in bulk water. Rates of chemical reactions in microdroplets for various chemical reactions, including condensation reactions, elimination reactions, protein unfolding, hydrogen−deuterium exchange, and substitution reactions, can be accelerated by factors of $\geq 10^3$ compared to that in bulk solution.[1−11] Thermodynamics of chemical reactions are also reported to be altered in microdroplets, enabling thermodynamically unfavorable reactions to proceed in microdroplets at room temperature.[12,13] Moreover, water microdroplets also induce the spontaneous reduction of organic molecules and metal ions, the formation of nanostructures without any added reducing agent or template,[14,15] and the formation of hydrogen peroxide.[16−18]

An electric field is long known to be able to profoundly affect chemical reactions,[19] including reaction product selectivity,[20−22] catalysis of reaction rates,[23,24] and redox reactions,[25] which could serve as one of the compelling mechanisms to account for the unusual properties of chemical reactions in aqueous microdroplets. Despite intensive efforts to estimate the strength of the electric field generated at the water surface that forms an interface with different media, considerable variation still exists in the calculated and measured values.[26] Moreover, the electric field is difficult to determine at the microdroplet surface, owing to several experimental challenges, including the required high imaging sensitivity and spatial resolution and the limited optical probes for reporting absolute electric field strength.

To directly study the electric field on the microdroplet, we coupled vibrational Stark spectroscopy[27] with recently developed stimulated Raman excited fluorescence (SREF) microscopy.[28,29] In SREF, the fluorescence excitation spectrum maps out the Raman line shape of the vibrational mode with superb sensitivity (up to single-molecule level). According to vibrational Stark spectroscopy, the vibrational frequency will be shifted by the amount $\Delta\nu$ by an external electric field F in a linear manner: $\Delta\nu = -\Delta\mu F$, where $\Delta\mu$ is known as the Stark tuning rate.[30] Hence, Stark-SREF imaging combines electric field sensing ability, ultrahigh detection sensitivity, and submicrometer spatial resolution obtained from all far-field optical geometry, rendering it ideal for this study.

We chose the dye molecule rhodamine 800 (Rh800) as the probe. It contains a conjugated nitrile group with its bond axis almost parallel to the permanent molecular dipole[31] (Figure 1a), allowing a good projection of the local electric field onto the vibrational bond axis. We prepared aqueous microdroplets containing 2 μM Rh800 enclosed by water-immiscible oils with ultrasonic emulsification of the mixture of Rh800 dissolved in water and hexadecane oil (details in the Supporting Information and Figure S1). A home-built two-photon excited fluorescence and SREF microscope was used for microdroplet imaging (Figure S2). The two-photon fluorescence imaging with the focal plane on the equator of the microdroplets shows localization of the probe near the microdroplet interface (Figure 1b,c) with an apparent enrichment factor of ∼200.

Received: July 5, 2020
Accepted: August 17, 2020
Published: August 17, 2020

https://dx.doi.org/10.1021/acs.jpclett.0c02061
J. Phys. Chem. Lett. 2020, 11, 7423−7428

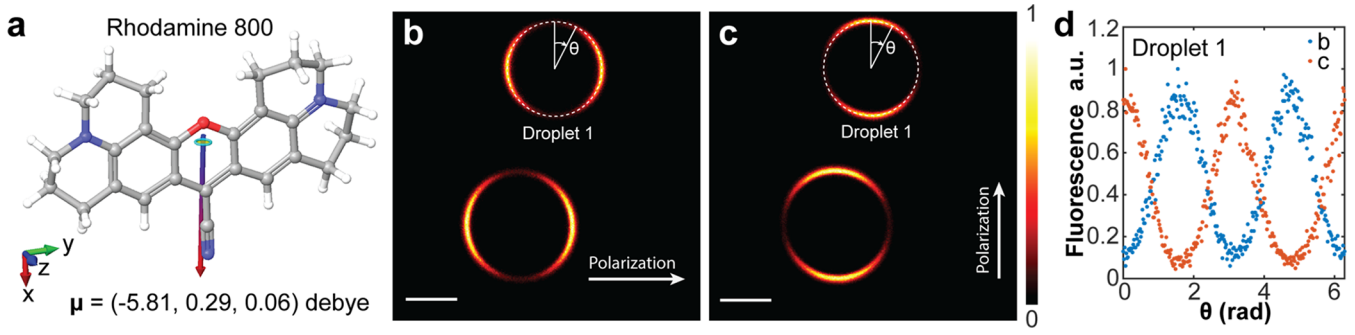

Figure 1. Two-photon fluorescence imaging of microdroplets in oil. (a) Structure of Rh800 and its dipole moment in vacuum calculated by Jaguar[31] with the B3LYP 6-311G**+ basis set. (b and c) Two-photon fluorescence images of microdroplets containing 2 μM Rh800 in hexadecane with two perpendicular excitation laser polarizations. (d) Normalized intensities of the fluorescence signals of droplet 1, labeled in panels b and c, as a function of the angle between the laser polarization direction (white arrow) and the viewing direction. Scale bar, 5 μm.

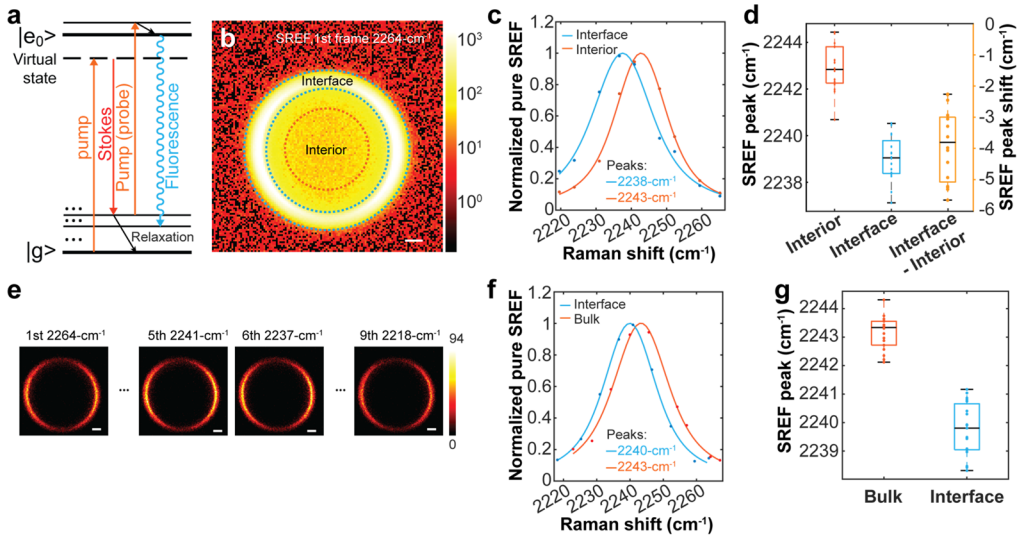

Figure 2. Stimulated Raman excited fluorescence (SREF) imaging of water microdroplets in oil. (a) Energy diagram of SREF. (b) First frame (excitation at 2264 cm^{-1}) of typical hyperspectral SREF imaging of the Rh800 nitrile mode of a water microdroplet (prepared with an initial concentration of 20 μM) in hexadecane. The intensity is displayed with a $\log_{10}$ scale; the color bar shows fluorescence counts (for a 0.4 ms pixel dwell time). (c) Background-subtracted SREF spectra of the Rh800 nitrile mode in the interior (red curve) and at the interface (blue curve) of the microdroplet in panel b (details in Figure S3). Red dots and blue dots represent the signal averages from the interior region (inside the red dashed circle in panel b) and from the interface region (between the blue dashed circles in panel b), respectively, of images collected at corresponding excitation wavenumbers; curves are the corresponding fitting results (details in Experimental methods in the Supporting Information). (d) Box plot of 16 independent measurements of the Rh800 nitrile peak position in the interior and at the interface and the corresponding Stark shift. (e) Typical hyperspectral SREF image series of microdroplets (prepared with an initial concentration of Rh800 molecules of 50 nM) in hexadecane and (f) corresponding typical background-subtracted SREF spectra of the microdroplet interface (blue curve) and a 20 μM Rh800 bulk water solution (red curve). (g) Box plot of the distribution of Rh800 nitrile peak positions for 18 measurements in bulk water and 19 measurements on the droplets prepared with a 50 nM Rh800 solution. Scale bar, 2 μm.

Subsequent studies examine this concentration enhancement effect in detail.[32] A large modulation depth (>90%) of the excitation anisotropy (Figure 1d) confirms that the dipole orientations of Rh800 molecules at the water−oil interface are rigidly aligned, which is consistent with observations described in a previous study.[33]

We performed two complementary sets of Stark-SREF measurements (Figure 2a) with different probe concentrations. As shown in panels b and c of Figure 1, the enrichment of dye molecules at the interface can deplete the probe in the interior of the microdroplets prepared in a micromolar solution. For a direct Stark shift estimation on the same droplet, we need to ensure a detectable SREF signal from both the interior and the interface. Thus, we increased the initial Rh800 concentration to 20 μM in our first experiment (Figure 2b). As a series of SREF images were scanned across the line shape of the nitrile mode, the SREF spectra of corresponding regions of each droplet were obtained. A clear red-shift of the nitrile peak was observed between the interface (blue curves, Figure 2c) and that of the interior region from typical droplets (red curve, Figure 2c and Figure S3a,b). Sixteen independent trails performed on different individual droplets yielded a red-shift of 4 ± 1 cm^{-1} (Figure 2d).

In the second set of measurements, a much lower Rh800 concentration (50 nM) was used to avoid potential perturbation by a high probe concentration (see Experimental methods in the Supporting Information and Figure 2e−g). Under these conditions, only the water−oil interface had detectable fluorescence. Hence, instead of comparing with the interior from the same droplets, we compared with a 20 μM

https://dx.doi.org/10.1021/acs.jpclett.0c02061
J. Phys. Chem. Lett. 2020, 11, 7423−7428

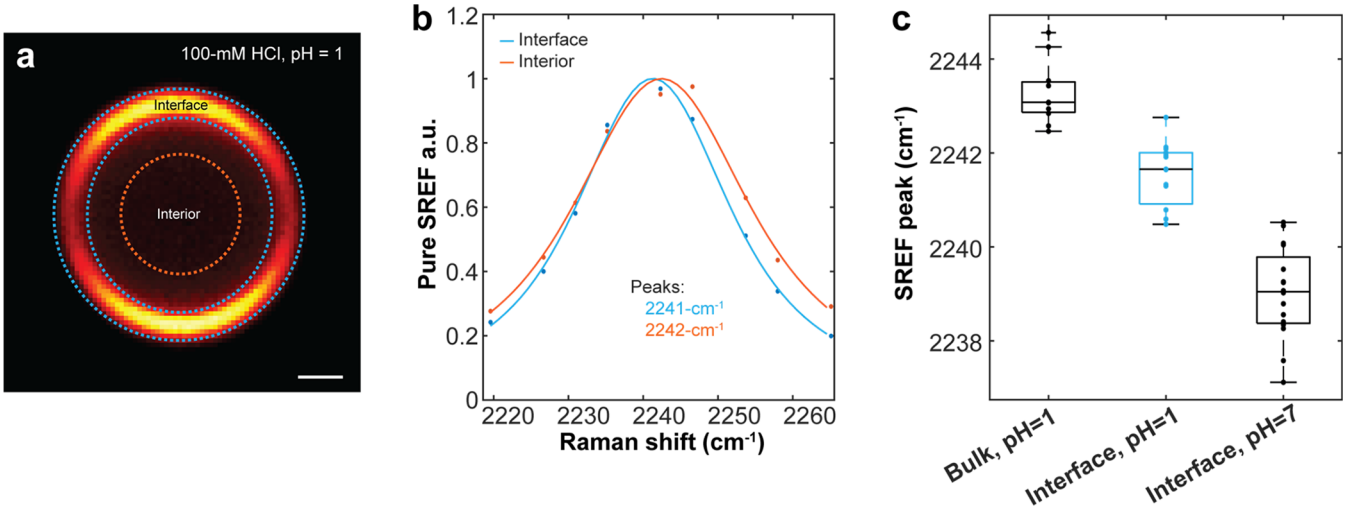

Figure 3. Perturbation by acid of the water−oil interface of microdroplets. (a) First frame (excitation at 2264 cm^{-1}) of typical hyperspectral SREF imaging of the Rh800 nitrile mode of a water microdroplet (prepared with an initial concentration of 20 μM in a 0.1 M HCl solution) in hexadecane. (b) Corresponding background-subtracted SREF spectra of the interface and interior regions. (c) Box plot of SREF peaks measured in the bulk 0.1 M HCl/20 μM Rh800 solution (pH 1), the droplet interface prepared with 10 μM Rh800 in a 0.1 M HCl solution (pH 1), and droplets prepared with 20 μM Rh800 (pH 7). Scale bar, 2 μm.

bulk Rh800 water solution prepared separately (Figure 2f and Figure S3c,d). Again, a red-shift of 3 ± 1 cm^{-1} was observed at the water−oil interface in 19 independent trials (Figure 2g), which is consistent with the result measured *in situ* (Figure 2d). Thus, the observed Stark shifts suggest the existence of a strong electric field at the microdroplet interface.

One may wonder whether added perchlorate ions, counterions of Rh800 probes, may contribute to the formation of the interfacial electric field. The experiment conducted with two different concentrations of Rh800 probes (20 μM for Figure 2b−d and 50 nM for Figure 2e−g) shows similar Stark shifts, suggesting that this effect is minimal. These comparisons also demonstrate that possible dye aggregation does not influence the observed Stark shift.

The nitrile mode of Rh800 has been calibrated to exhibit a $\Delta\mu$ of ∼0.53 ± 0.09 cm^{-1}/(MV/cm) based on vibrational solvatochromic measurements and Onsager reaction field theory.[34] This value is very close to the reported $\Delta\mu$ of 0.61 cm^{-1}/(MV/cm) for aromatic nitriles determined via infrared spectroscopy.[35] Therefore, the 4 cm^{-1} red-shift at the oil−water interface of microdroplet indicates a local electrostatic field of ∼8 MV/cm. Besides the hexadecane experiment described above, SREF measurements of water microdroplets formed in other oils were also investigated. Figure S4 shows the result in silicone oils of varying viscosities from different vendors, and comparable red-shifts ranging from 3 ± 1 to 5 ± 1 cm^{-1} were also observed. In addition, no obvious dependence on microdroplet size was observed from microdroplets between 4 and 20 μm in diameter under the current spectral resolution (∼1 cm^{-1}) (Figure 2 and Figure S4). Together, these results support the existence of the strong electrostatic field on the order of ∼10^7 V/cm as experienced by the probe molecule at the microdroplet water−oil interface. Note that what we measure here is a local electric field experienced by the probe molecule, which has contributions from the electric field arising from the double layer as well as the effect of this electric field on the solvent H_2O molecules in the double layer, which in turn influences their intimate interactions (such as hydrogen bonding) with the probe molecule.

Unlike organic solvents, water promotes ionization and itself ionizes into hydroxide (OH^-) and hydronium (H_3O^+) ions. Although this topic remains controversial,[36,37] many studies indicate that the surface of water droplets is negatively charged.[38,39] A pH-dependent study of surfactant-free oil emulsion droplets in water showed that the autolyzed hydroxide ions charge the water−oil interface and stabilize droplets.[40] Tian and Shen using phase-sensitive sum frequency vibrational spectroscopy showed that the OH^- has the highest adsorption energy compared to those of H_3O^+ and Cl^- at a water−silane interface.[41] A study with second harmonic generation spectroscopy showed that hydroxide ions exhibit affinity for the water−oil interface.[42] Wu et al. used second harmonic generation spectroscopy to report that the water−oil interface is negatively charged and described the role of the interfacial electric field in particle adsorption.[43] A claim has been made that this negative charging is caused by the preferential adsorption of OH^- to the hydrophobic interface in which H^+ is solvated more strongly than OH^-, although scrupulously purified water nanodroplets appear to have little to no charge.[44] A recent review suggests that the presence of trace impurities in water likely dominates in determining the sign of the charge on the droplet periphery, and they are most often believed to be anionic surfactants of unknown composition.[45] However, claims about the preferential adsorption of positive ions at the water surface do exist. Devlin, Jungwirth, and co-workers argued from molecular dynamics simulations that the periphery of water droplets is not basic but rather acidic, based on the results that showed a preference for hydronium ions to be on the interface rather than hydroxide ions.[46] This claim has been supported by the study of Voth and co-workers on H^+ clustering at the water surface.[47] Whatever ions are present, it is unlikely that the cations and anions have identical affinities for the oil−water interface. Such different affinities for the interface would give rise to charge separation and the formation of a double layer.[48−50] This model could generate an electric field to align

https://dx.doi.org/10.1021/acs.jpclett.0c02061
J. Phys. Chem. Lett. 2020, 11, 7423−7428

the probe orientations and water molecules and to confine the translational motion into a two-dimensional thin layer at the water−oil interface.

To examine this hypothesis that the electric field was formed from the separation of charges between negative ions at the microdroplet interface and positive ions inside the water microdroplet near the interface, we added acid to microdroplets and measured the magnitude of the Stark shift at the water−oil interface. Figure 3 shows that the Stark shift drops to 1 ± 1 cm^{-1} for the microdroplets prepared in a 0.1 M HCl solution (pH 1). Introducing H^+ acts to neutralize the concentration of negatively charged ions, such as OH^- or other anionic species on the microdroplet periphery. The SREF peak measured in bulk aqueous solution at pH 1 (Figure 3c) remained unchanged compared to that of the bulk solution at pH 7 (Figure 2g), showing that the Stark shift was not influenced by added HCl. In addition, we examined whether the reduction of the Stark shift upon addition of HCl to microdroplets was caused by Cl^- ions. We conducted a control experiment by measuring the Stark shift in aqueous microdroplets prepared in a 0.1 M NaCl solution. There was no difference in the Stark shift between the microdroplet interface in 0.1 M NaCl (Figure S5) compared to the microdroplet interface at pH 7 (Figure 2c). These data confirm that the acid-induced Stark shift was not caused by Cl^- ions. Therefore, this result supports the idea that it is the high affinity of negatively charged ions for the interface that creates a strong electric field at the microdroplet water−oil interface. Moreover, it also establishes experimentally the sign of the observed electric field at the interface for water microdroplets in oil that we have prepared.

We speculate that one of the unknown anionic surfactants might be the bicarbonate anion (HCO_3^-) arising from dissolved atmospheric carbon dioxide (CO_2) in the water microdroplet from contact with air. To test this hypothesis, we bubbled CO_2 through the water prior to ultrasonication forming microdroplets, and we found a small increase in the Stark shift of Rh800 at the microdroplet periphery from ∼4 ± 1 to 5 ± 1 cm^{-1} (see Figure S6). This finding suggests that dissolved carbon dioxide might be one factor contributing to why the oil−water interface of the microdroplet is negatively charged and develops a strong electric field. Clearly, more work is needed to definitively identify the ionic surfactant identity or identities, but the work presented here unquestionably establishes the existence and sign of a large electric field at the water microdroplet periphery.

In light of the structure−function relationship, our observation of a strong electric field at the interface of aqueous microdroplets may shed light on the emerging field of microdroplet chemistry.[1−10,12−18] It has been documented that many reactions involving charged or polar species can be accelerated by a factor of $\geq 10^3$ inside microdroplets.[11] Indeed, the rates of acid-catalyzed or base-catalyzed reactions are markedly enhanced for water microdroplets.[3,8] Our measured field strength as experienced by the probe on the order of a few MV/cm might directly affect the reaction transition state, as an MV/cm-level external field acting on aligned reactant molecules is reported to significantly change the energy profile of chemical reactions,[19] resulting in reaction product selectivity[20−22] and catalysis of reactions.[23,24] Several previous theoretical calculations showed the existence of the interfacial potential at the water surface. Cendagorta and Ichiye reported the formation of a water−vapor interface potential as high as 0.4 V with the corresponding electric field at 8 MV/cm, which originates from the aligned orientation of water dipoles at the interface.[51] Quasichemical theory showed the dominant role of the solvent molecular quadrupole for the formation of interfacial potential and an electric field as strong as 1 MV/cm.[52] Leung used density functional theory to estimate the water surface potential and the interfacial electric field to be approximately 3.63 V and 10 MV/cm, respectively.[53] Another study by Kathmann and co-workers reported that a peak field of 150 MV/cm is estimated at the water−air interface by an *ab initio* molecular dynamics simulation.[54] These studies mostly attribute the formation of the interfacial electric field to the ordered orientation of water molecules at the water surface, which is related to the mechanism proposed in this work. Several studies using vibrational sum frequency generation spectroscopy reported free dangling OH[55,56] and an ordered water layer at the water−hydrophobic interface.[57] We currently do not have enough empirical evidence that either supports or refutes these different views, which remain to be further studied. In any case, the measured value of the interfacial electric field strength by the SREF measurement is in rough agreement with previous calculations. A strong field amplitude (≥10 MV/cm) may support the removal of bonded electrons and induce spontaneous oxidations[16−18] and reductions[14,15] observed in aqueous microdroplets. The electric field also provides an elucidation of the alignment of molecules near the interface[58] and consequently minimized the entropic barrier of chemical reactions in microdroplets.[12,13]

■ ASSOCIATED CONTENT

Supporting Information

The Supporting Information is available free of charge at https://pubs.acs.org/doi/10.1021/acs.jpclett.0c02061.

Experimental methods and Figures S1−S6 (PDF)

■ AUTHOR INFORMATION

Corresponding Authors

Richard N. Zare − *Department of Chemistry, Stanford University, Stanford, California 94305, United States;* orcid.org/0000-0001-5266-4253; Email: zare@stanford.edu

Wei Min − *Department of Chemistry, Columbia University, New York, New York 10027, United States;* orcid.org/0000-0003-2570-3557; Email: wm2256@columbia.edu

Authors

Hanqing Xiong − *Department of Chemistry, Columbia University, New York, New York 10027, United States*

Jae Kyoo Lee − *Department of Chemistry, Stanford University, Stanford, California 94305, United States*

Complete contact information is available at: https://pubs.acs.org/10.1021/acs.jpclett.0c02061

Notes

The authors declare no competing financial interest.

■ ACKNOWLEDGMENTS

The authors thank Y. Miao, N. Qian, L. Shi, Y. Yang, and F. Hu for helpful discussions and are grateful for financial support from National Institutes of Health Grant R01 GM132860 and National Science Foundation Grant CHE-1904684 (to W.M.)

and Air Force Office of Scientific Research AFOSR FA9550-16-1-0113 (to R.N.Z.).

REFERENCES

(1) Lee, J. K.; Kim, S.; Nam, H. G.; Zare, R. N. Microdroplet fusion mass spectrometry for fast reaction kinetics. *Proc. Natl. Acad. Sci. U. S. A.* **2015**, *112* (13), 3898−3903.

(2) Lee, J. K.; Banerjee, S.; Nam, H. G.; Zare, R. N. Acceleration of reaction in charged microdroplets. *Q. Rev. Biophys.* **2015**, *48* (4), 437−444.

(3) Banerjee, S.; Zare, R. N. Syntheses of isoquinoline and substituted quinolines in charged microdroplets. *Angew. Chem., Int. Ed.* **2015**, *54* (49), 14795−14799.

(4) Badu-Tawiah, A.; Campbell, D.; Cooks, R. G. Accelerated C-N Bond Formation in Dropcast Thin Films on Ambient Surfaces. *J. Am. Soc. Mass Spectrom.* **2012**, *23* (9), 1461−1468.

(5) Bain, R. M.; Pulliam, C. J.; Cooks, R. G. Accelerated Hantzsch electrospray synthesis with temporal control of reaction intermediates. *Chem. Sci.* **2015**, *6* (1), 397−401.

(6) Fallah-Araghi, A.; Meguellati, K.; Baret, J.-C.; Harrak, A. E.; Mangeat, T.; Karplus, M.; Ladame, S.; Marques, C. M.; Griffiths, A. D. Enhanced Chemical Synthesis at Soft Interfaces: A Universal Reaction-Adsorption Mechanism in Microcompartments. *Phys. Rev. Lett.* **2014**, *112* (2), 028301.

(7) Girod, M.; Moyano, E.; Campbell, D. I.; Cooks, R. G. Accelerated bimolecular reactions in microdroplets studied by desorption electrospray ionization mass spectrometry. *Chem. Sci.* **2011**, *2* (3), 501.

(8) Müller, T.; Badu-Tawiah, A.; Cooks, R. G. Accelerated Carbon-Carbon Bond-Forming Reactions in Preparative Electrospray. *Angew. Chem., Int. Ed.* **2012**, *51* (47), 11832−11835.

(9) Lee, J. K.; Nam, H. G.; Zare, R. N. Microdroplet fusion mass spectrometry: accelerated kinetics of acid-induced chlorophyll demetallation. *Q. Rev. Biophys.* **2017**, *50*, e2.

(10) Jansson, E. T.; Lai, Y.-H.; Santiago, J. G.; Zare, R. N. Rapid hydrogen-deuterium exchange in liquid droplets. *J. Am. Chem. Soc.* **2017**, *139* (20), 6851−6854.

(11) Wei, Z.; Li, Y.; Cooks, R. G.; Yan, X. Accelerated Reaction Kinetics in Microdroplets: Overview and Recent Developments. *Annu. Rev. Phys. Chem.* **2020**, *71*, 31−51.

(12) Nam, I.; Lee, J. K.; Nam, H. G.; Zare, R. N. Abiotic production of sugar phosphates and uridine ribonucleoside in aqueous microdroplets. *Proc. Natl. Acad. Sci. U. S. A.* **2017**, *114*, 12396.

(13) Nam, I.; Nam, H. G.; Zare, R. N. Abiotic synthesis of purine and pyrimidine ribonucleosides in aqueous microdroplets. *Proc. Natl. Acad. Sci. U. S. A.* **2018**, *115*, 36.

(14) Lee, J. K.; Samanta, D.; Nam, H. G.; Zare, R. N. Micrometer-Sized Water Droplets Induce Spontaneous Reduction. *J. Am. Chem. Soc.* **2019**, *141* (27), 10585−10589.

(15) Lee, J. K.; Samanta, D.; Nam, H. G.; Zare, R. N. Spontaneous formation of gold nanostructures in aqueous microdroplets. *Nat. Commun.* **2018**, *9* (1), 1562.

(16) Lee, J. K.; Walker, K. L.; Han, H. S.; Kang, J.; Prinz, F. B.; Waymouth, R. M.; Nam, H. G.; Zare, R. N. Spontaneous generation of hydrogen peroxide from aqueous microdroplets. *Proc. Natl. Acad. Sci. U. S. A.* **2019**, *116* (39), 19294−19298.

(17) Gao, D.; Jin, F.; Lee, J. K.; Zare, R. N. Aqueous microdroplets containing only ketones or aldehydes undergo Dakin and Baeyer-Villiger reactions. *Chem. Sci.* **2019**, *10* (48), 10974−10978.

(18) Dulay, M. T.; Lee, J. K.; Mody, A. C.; Narasimhan, R.; Monack, D. M.; Zare, R. N. Spraying Small Water Droplets Acts as a Bacteriocide. *Quarterly Review of Biophysics Discovery* **2020**, *1*, DOI: 10.1017/qrd.2020.2.

(19) Shaik, S.; Ramanan, R.; Danovich, D.; Mandal, D. Structure and reactivity/selectivity control by oriented-external electric fields. *Chem. Soc. Rev.* **2018**, *47* (14), 5125−5145.

(20) Shaik, S.; de Visser, S. P.; Kumar, D. External electric field will control the selectivity of enzymatic-like bond activations. *J. Am. Chem. Soc.* **2004**, *126* (37), 11746−11749.

(21) Huang, X.; Tang, C.; Li, J.; Chen, L.-C.; Zheng, J.; Zhang, P.; Le, J.; Li, R.; Li, X.; Liu, J.; et al. Electric field-induced selective catalysis of single-molecule reaction. *Sci. Adv.* **2019**, *5* (6), No. eaaw3072.

(22) Gorin, C. F.; Beh, E. S.; Kanan, M. W. An Electric Field-Induced Change in the Selectivity of a Metal Oxide-Catalyzed Epoxide Rearrangement. *J. Am. Chem. Soc.* **2012**, *134* (1), 186−189.

(23) Meir, R.; Chen, H.; Lai, W.; Shaik, S. Oriented electric fields accelerate Diels-Alder reactions and control the endo/exo selectivity. *ChemPhysChem* **2010**, *11* (1), 301−310.

(24) Aragonès, A. C.; Haworth, N. L.; Darwish, N.; Ciampi, S.; Bloomfield, N. J.; Wallace, G. G.; Diez-Perez, I.; Coote, M. L. Electrostatic catalysis of a Diels-Alder reaction. *Nature* **2016**, *531* (7592), 88.

(25) Sakamaki, M.; Amemiya, K. Observation of an electric field-induced interface redox reaction and magnetic modification in GdO x/Co thin film by means of depth-resolved X-ray absorption spectroscopy. *Phys. Chem. Chem. Phys.* **2018**, *20* (30), 20004−20009.

(26) Paluch, M. Surface potential at the water-air interface. *Ann. Univ. Mariae Curie-Sklodowska, Sect. AA: Chem.* **2016**, *70* (2), 1.

(27) Bublitz, G. U.; Boxer, S. G. Stark spectroscopy: applications in chemistry, biology, and materials science. *Annu. Rev. Phys. Chem.* **1997**, *48* (1), 213−242.

(28) Xiong, H.; Shi, L.; Wei, L.; Shen, Y.; Long, R.; Zhao, Z.; Min, W. Stimulated Raman excited fluorescence spectroscopy and imaging. *Nat. Photonics* **2019**, *13* (6), 412.

(29) Xiong, H.; Qian, N.; Miao, Y.; Zhao, Z.; Min, W. Stimulated Raman Excited Fluorescence Spectroscopy of Visible Dyes. *J. Phys. Chem. Lett.* **2019**, *10* (13), 3563−3570.

(30) Fried, S. D.; Boxer, S. G. Measuring electric fields and noncovalent interactions using the vibrational Stark effect. *Acc. Chem. Res.* **2015**, *48* (4), 998−1006.

(31) Bochevarov, A. D.; Harder, E.; Hughes, T. F.; Greenwood, J. R.; Braden, D. A.; Philipp, D. M.; Rinaldo, D.; Halls, M. D.; Zhang, J.; Friesner, R. A. Jaguar: A high-performance quantum chemistry software program with strengths in life and materials sciences. *Int. J. Quantum Chem.* **2013**, *113* (18), 2110−2142.

(32) Xiong, H.; Lee, J. K.; Zare, R. N.; Min, W. Strong Concentration Enhancement of Charged Molecules at the Interface of Aqueous Microdroplets, under preparation.

(33) Zhou, Z.; Yan, X.; Lai, Y.-H.; Zare, R. N. Fluorescence Polarization Anisotropy in Microdroplets. *J. Phys. Chem. Lett.* **2018**, *9* (11), 2928−2932.

(34) Shi, L.; Hu, F.; Min, W. Optical mapping of biological water in single live cells by stimulated Raman excited fluorescence microscopy. *Nat. Commun.* **2019**, *10* (1), 4764.

(35) Bagchi, S.; Fried, S. D.; Boxer, S. G. A solvatochromic model calibrates nitriles' vibrational frequencies to electrostatic fields. *J. Am. Chem. Soc.* **2012**, *134* (25), 10373−10376.

(36) Saykally, R. J. Air/water interface: Two sides of the acid-base story. *Nat. Chem.* **2013**, *5* (2), 82.

(37) Agmon, N.; Bakker, H. J.; Campen, R. K.; Henchman, R. H.; Pohl, P.; Roke, S.; Thämer, M.; Hassanali, A. Protons and hydroxide ions in aqueous systems. *Chem. Rev.* **2016**, *116* (13), 7642−7672.

(38) Roger, K.; Cabane, B. Why are hydrophobic/water interfaces negatively charged? *Angew. Chem., Int. Ed.* **2012**, *51* (23), 5625−5628.

(39) Beattie, J. K.; Djerdjev, A. M.; Warr, G. G. The surface of neat water is basic. *Faraday Discuss.* **2009**, *141*, 31−39.

(40) Beattie, J. K.; Djerdjev, A. M. The pristine oil/water interface: Surfactant-free hydroxide-charged emulsions. *Angew. Chem., Int. Ed.* **2004**, *43* (27), 3568−3571.

(41) Tian, C.; Shen, Y. Structure and charging of hydrophobic material/water interfaces studied by phase-sensitive sum-frequency vibrational spectroscopy. *Proc. Natl. Acad. Sci. U. S. A.* **2009**, *106* (36), 15148−15153.

(42) Gan, W.; Wu, W.; Yang, F.; Hu, D.; Fang, H.; Lan, Z.; Yuan, Q. The behavior of hydroxide and hydronium ions at the hexadecane-water interface studied with second harmonic generation and zeta potential measurements. *Soft Matter* **2017**, *13* (43), 7962−7968.

https://dx.doi.org/10.1021/acs.jpclett.0c02061
J. Phys. Chem. Lett. 2020, 11, 7423−7428

(43) Wu, W.; Liu, X.; Chen, S.-L.; Yuan, Q.; Gan, W. Particle adsorption at the oil-water interface studied with second harmonic generation. *Soft Matter* **2019**, *15* (38), 7672−7677.
(44) Carpenter, A. P.; Tran, E.; Altman, R. M.; Richmond, G. L. Formation and surface-stabilizing contributions to bare nano-emulsions created with negligible surface charge. *Proc. Natl. Acad. Sci. U. S. A.* **2019**, *116* (19), 9214−9219.
(45) Uematsu, Y.; Bonthuis, D. J.; Netz, R. R. Impurity effects at hydrophobic surfaces. *Current Opinion in Electrochemistry* **2019**, *13*, 166−173.
(46) Buch, V.; Milet, A.; Vácha, R.; Jungwirth, P.; Devlin, J. P. Water surface is acidic. *Proc. Natl. Acad. Sci. U. S. A.* **2007**, *104* (18), 7342−7347.
(47) Burnham, C. J.; Petersen, M. K.; Day, T. J.; Iyengar, S. S.; Voth, G. A. The properties of ion-water clusters. II. Solvation structures of Na+, Cl-, and H+ clusters as a function of temperature. *J. Chem. Phys.* **2006**, *124* (2), 024327.
(48) Israelachvili, J. N. *Intermolecular and surface forces*; Academic Press, 2015.
(49) Chamberlayne, C. F.; Zare, R. N. Simple model for the electric field and spatial distribution of ions in a microdroplet. *J. Chem. Phys.* **2020**, *152*, 184702−184707.
(50) Kwan, V.; Consta, S. Bridging electrostatic properties between nanoscopicand microscopic highly charged droplets. *Chem. Phys. Lett.* **2020**, *746*, 137238−137245.
(51) Cendagorta, J. R.; Ichiye, T. The surface potential of the water-vapor interface from classical simulations. *J. Phys. Chem. B* **2015**, *119* (29), 9114−9122.
(52) Doyle, C. C.; Shi, Y.; Beck, T. L. The importance of the water molecular quadrupole for estimating interfacial potential shifts acting on ions near the liquid-vapor interface. *J. Phys. Chem. B* **2019**, *123* (15), 3348−3358.
(53) Leung, K. Surface potential at the air- water interface computed using density functional theory. *J. Phys. Chem. Lett.* **2010**, *1* (2), 496−499.
(54) Kathmann, S. M.; Kuo, I.-F. W.; Mundy, C. J. Electronic Effects on the Surface Potential at the Vapor- Liquid Interface of Water. *J. Am. Chem. Soc.* **2009**, *131* (47), 17522−17522.
(55) Richmond, G. Molecular bonding and interactions at aqueous surfaces as probed by vibrational sum frequency spectroscopy. *Chem. Rev.* **2002**, *102* (8), 2693−2724.
(56) Björneholm, O.; Hansen, M. H.; Hodgson, A.; Liu, L.-M.; Limmer, D. T.; Michaelides, A.; Pedevilla, P.; Rossmeisl, J.; Shen, H.; Tocci, G.; et al. Water at interfaces. *Chem. Rev.* **2016**, *116* (13), 7698−7726.
(57) Tyrode, E.; Liljeblad, J. F. Water structure next to ordered and disordered hydrophobic silane monolayers: a vibrational sum frequency spectroscopy study. *J. Phys. Chem. C* **2013**, *117* (4), 1780−1790.
(58) Cristadoro, A.; Ai, M.; Räder, H. J.; Rabe, J. P.; Müllen, K. Electrical field-induced alignment of nonpolar hexabenzocoronene molecules into columnar structures on highly oriented pyrolitic graphite investigated by STM and SFM. *J. Phys. Chem. C* **2008**, *112* (14), 5563−5566.

https://dx.doi.org/10.1021/acs.jpclett.0c02061
J. Phys. Chem. Lett. 2020, 11, 7423−7428